HHS Public Access

Author manuscript

Photochem Photobiol. Author manuscript; available in PMC 2021 March 01.

Published in final edited form as:

Photochem Photobiol. 2020 March ; 96(2): 365–372. doi:10.1111/php.13191.

Modulation of extracellular matrix rigidity via riboflavin-mediated photocrosslinking regulates invasive motility and treatment response in a 3D pancreatic tumor model

Rojin Jafari[1], **Gwendolyn M. Cramer**[1,2], **Jonathan P. Celli**[1,*]

[1]Department of Physics, University of Massachusetts Boston

[2]Molecular, Cellular and Organismal Biology (MCOB) Program, University of Massachusetts Boston

Abstract

In this study we evaluate the use of riboflavin-mediated collagen photocrosslinking as an experimental tool to modulate extracellular matrix (ECM) mechanical properties in 3D in vitro tumor models. Using this approach in conjunction with 3D pancreatic tumor spheroid transplants, we show that the extent of matrix photocrosslinking in reconstituted hydrogels with fixed protein concentration scales inversely with the extent of invasive progression achieved by cells infiltrating into the surrounding ECM from primary transplanted spheroids. Using cross-linking to manipulate the extent of invasion into ECM in conjunction with imaging-based treatment assessment, we further leverage this approach as a means for assaying differential therapeutic response in primary nodule and ECM-invading populations and compare response to verteporfin-based photodynamic therapy (PDT) and oxaliplatin chemotherapy. Treatment response data shows that invading cell populations (which also exhibit markers of increased EMT) are highly chemoresistant yet have significantly increased sensitivity to PDT relative to the primary nodule. In contrast, the oxaliplatin treatment achieves greater growth inhibition of the primary nodule. These findings may be significant in themselves, while the methodology developed here could have a broader range of applications in developing strategies to target invasive disease and/or mecahanobiological determinants of therapeutic response in solid tumors.

INTRODUCTION

Tumor growth and progression is determined not only by the biology of malignant cells, but also by how they interact with their microenvironment. In particular the importance of the physical properties of the tumor microenvironment have become increasingly recognized (1-3). Many solid tumors are associated with dense fibrous extracellular matrix (ECM) (4). In this fibrous ECM, Type I collagen (COL1) is a key component contributing to the mechanical properties of the tumor microenvironment, which in turn has been shown to regulate growth and invasive behavior of cancer cells (5-7). For example, in a pioneering study by Paszek et al it was shown that increased substrate rigidity itself can perturb epithelial morphogenesis and promote malignant behavior (3). This may be particularly

*Corresponding author jonathan.celli@umb.edu.

relevant for tumors of the pancreas (used as an exemplar model system in this study) which are noted for a profound desmoplastic reaction and as much as 80 to 90% fibrotic stroma content (8-10).

The role of local tissue mechanics, and in particular the properties of collagen ECM, in regulating tumor growth behavior is a topic which has received significant attention in the literature (11, 1, 12). ECM which is rich in COL1 is found to promote invasive behavior as compared to laminin-rich ECM (13, 5), though the details of how matrix stiffness regulate motility are complex. On the one hand external compressive stress (14), and stiffness (15-17) activate invasive behavior, yet softer ECM may be more conducive to achieving invasive motility (18). To investigate this, the need for designing experimental tumor model systems with tunable mechanical properties, independent of the biochemical composition has motivated numerous studies either with synthetic materials or addition of biologically inert components that increase stiffness of ECM hydrogels with fixed protein concentration (19-21, 11).

In this study we explore the possibility of using riboflavin (RF)-mediated photocrosslinking of collagen as a means to modulate ECM mechanics, and subsequent impact on invasive behavior and response to treatments, in a pancreatic 3D tumor model. The implementation of riboflavin photochemistry to catalyze formation of COL1 crosslinks is well characterized, and has been explored in numerous applications including clinical use in crosslinking of corneal collagen for treatment of progressive keratoconus (22-27). In the present study we specifically leverage the capability to manipulate ECM rheology via photocrosslinking as a means to study how activation of invasive behavior impacts upon responsiveness to chemotherapy and photodynamic therapy (PDT). This line of investigation is motivated by our previous study using transplanted 3D pancreatic tumor spheroids in collagen and laminin-rich ECM which promote and constrain, respectively, the invasive progression of peripheral cells of the primary spheroid into surrounding ECM (13). We found that ECM-infiltrating cells exhibit increased sensitivity to PDT, yet decreased response to chemo, which is also consistent with evidence of increased epithelial-mesenchymal transition (EMT) in invading cells. While in the previous study the invasive behavior of cancer cells was regulated by the combined influence mechanical properties and composition of the ECM, the use of photocrosslinking here allows the tuning of rigidity using the same concentration of the same ECM protein (COL1).

Here we begin by reporting rheological characterization of reconstituted COL1 hydrogels with varying extent of RF-induced photocrosslinking using standard frequency-dependent bulk oscillatory shear rheology measurements. We then explore how ECM mechanics impacts on phenotype of pancreatic tumor spheroids transplanted into COL1 ECM, in particular focusing on invasive behavior and motility. Finally, having established conditions which give rise to calibrated extent of invasive progression into the ECM, we investigate treatment response to chemotherapy (using oxaliplatin) and PDT (using verteporfin) in both the primary transplanted spheroid and the ECM-infiltrating cell populations. Given the selection of specific therapeutics investigated here are motivated by relevant to clinical treatment for pancreatic cancer, which increasingly uses the FOLFIRINOX regimen for patients who can tolerate the toxicity of this multi-drug cocktail (of which oxaliplatin is a

key component) (28). The investigation of verteporfin for invasive pancreatic cancer is motivated by clinical research which has shown promise and established safety and feasibility of verteporfin PDT for treatment of pancreatic cancer (29).

MATERIALS AND METHODS

Cell Culture and Reagents:

PANC1 cell lines were obtained from the American Type Culture Collection (Manassas, VA), and grown in T-75 cell culture flasks according to ATTC guidelines. DMEM (HyClone; Logan, UT) were supplemented with 10% FBS (HyClone; Logan, UT), 100 IU/mL penicillin and 1% streptomycin (HyClone; Logan, UT), and 0.5 ug/mL Amphotericin B (Corning; Corning, NY). Cell lines were passaged a maximum of 25 times before discarding and thawing cryogenically stored stocks.

Rheology of Photocrosslinked collagen hydrogels:

Collagen 1 (COL1) solutions were initially prepared from Type I collagen (High Concentration Rat Tail Collagen, Corning™ product number 354249) in 10x MEM (Sigma-Aldrich; St. Louis, MO) and sterile cell culture grade water (HyClone; Logan, UT), adjusted to a neutral pH (7.2-7.6) with NaOH 1N (Fisher Chemical; Pittsburgh, PA) in tubes immersed in an ice bath. Aliquots of 440 uL of these solutions were prepared to a concentration of 3.7 mg/ml with 0.1% riboflavin (RF) (from 5mM solution of riboflavin-5-monophosphate (TCI America, Portland, OR) or without RF for relevant control groups in which case the RF volume was offset with additional sterile water. The RF concentration used here is informed by previous collagen photocrosslinking studies (25, 30, 31, 26, 23, 32, 27). For rheology studies, samples were prepared in 60mm petri dishes (BioLite, Rochester, NY). Samples in solution phase were exposed to blue light (THORLABS M450LP1, Blue LED) positioned 2.5 cm above and calibrated to an irradiance of approximately 420 mW/cm^2 for durations of 2 to 236 seconds to achieve specified total light doses of 0.5 to 100 J/cm2. As shown in Figure 1A measurement of spectral output of device and the RF absorption spectrum have excellent agreement. In preliminary experiment various light sources were evaluated for COL I/RF photocrosslinking including blue LED flash light, dental curing light (25) (Rainbow Blue LED Curing Light), Blue PAR38 LED (Feit Electric, Pico Rivera, CA) and THORLABS M450LP1, respectively though the latter source was ultimately selected as the most robust, stable and tunable and was used for all data reported here. Control groups with only riboflavin (PS only), no light and no riboflavin (NL/NPS) and light only (LO; using highest fluence administered in the experiment) were also included. After light exposure dishes of collagen were incubated without media at a humidified atmosphere at 37°C and 5% CO2 to allow gelation at varying extent of crosslinking to proceed for approximately 16 hours.

For rheological characterization the dishes containing photocrosslinked (or control) samples were transferred to a Discovery Hybrid Rheometer (TA Instruments, New Castle Delaware) fitted with a stainless steel 40 mm perforated parallel plate. As samples were placed on the rheometer with the 60 mm petri dish, prior to every measurement, gap was zeroed with an empty petri dish on the rheometer metal at 37°C. After allowing 10 minutes for samples to

equilibrate, the frequency-dependent storage and loss moduli, $G'(\omega)$ and $G''(\omega)$ respectively, for each collagen sample were measured. Briefly, for oscillatory shear deformation in the linear regime, the storage modulus, $G'(\omega)$, reports the component of stress in phase with strain in the material and is related to elastic energy storage. The loss modulus, $G''(\omega)$, reports the component of stress out of phase with the strain and is related to the viscosity of the material. The linear regime for each sample was initially assessed by running oscillation amplitude sweeps at a constant temperature of 37°C, frequency of 0.15 Hz (0.9 rad/s), strain of 0.1-2% and a gap size of 340 um (optimal filling gap for the spread of sample with parallel plate geometry). An appropriate strain value in the linear regime was selected for subsequent frequency sweep runs over a range of $1 < \omega < 100$ rad/s. Following initial non-destructive characterization of linear viscoelastic response, a second amplitude sweep was conducted to examine yield properties of the material.

3D tumor spheroid preparation:

PANC1 tumor spheroids were formed on agarose menisci in 96-well plates as an attachment free surface as described previously (13, 33). Briefly, spheroids were formed from suspensions of 200 cells per 100 uL plated on the surface of agarose menisci (protein electrophoresis grade agarose, Fisher BioReagents) that were formed in advance in 96 well plates by adding 48 uL per well 1% heated agarose and allowing to set at room temperature for 30 minutes. Multicellular spheroids were supplemented with media containing 2% GFR (Growth Factor Reduced) Matrigel (Corning; Corning, NY) after 24 hours and replenished after 3 days.

Photocrosslinking of Collagen 3D cultures:

In situ cross-linking of collagen around transplanted 3D spheroids used identical irradiance and preparation to that for rheological characterization but in multiwell plate format instead of dishes. Type I collagen from rat tail (Corning™ 354249) prepared previously in 10x MEM (Sigma-Aldrich; St. Louis, MO) and sterile cell culture water and adjusted to a neutral pH (7.2-7.6) with NaOH 1N (Fisher Chemical; Pittsburgh, PA) as described above. As specified in the text, spheroids were either transplanted immediately before or immediately after irradiation (while still in solution phase). In either case spheroids were grown for 7 days prior to transplantation then collected in their growth media and incorporated into collagen on ice to a final concentration of 3.7 mg/ml COL I containing 0.1% riboflavin (or without riboflavin) and transferred to chilled 24 well black-walled plate (ibidi USA Inc.; Madison, WI) for photocrosslinking. Only spheroids that were successfully transplanted intact were included for subsequent analysis (to avoid any artifacts from cells mechanically sheared off from pipetting being counted as invading cells). The plate was placed on a plexi glass stage with the blue LED (THORLABS M450LP1) positioned 2.5 cm below as shown in Figure 1B. The blue light irradiance of 420mW/cm^2 reached the well through a hole on the plexi glass slightly overfilling one well without delivering to neighboring wells. (Note: For preparation of samples for rheology the light was delivered to dishes from above, rather than below in the case of multiwell dishes used for 3D cultures). Depending on growth condition assignment wells were prepared in triplicate to receive either no light/no riboflavin, riboflavin only, light only (15 J/cm^2), or photocrosslinking with riboflavin/light (0.5, 10 and 15 J/cm^2). After irradiation, culture plates were incubated without media at a

humidified atmosphere at 37°C and 5% CO_2 for 16 hours (as for rheology measurements), before topping each well with 400uL complete media.

Image-based quantification of ECM invasion:

Transplanted spheroids were allowed to grow and invade into photo-crosslinked (or control) ECM for 6 days. To evaluate invasive progression, on day 6 cultures were terminally stained with vital dyes calcein AM (ThermoFisher Scientific Molecular Probes; Waltham, MA) and ethidium bromide (Fisher BioReagents; Pittsburgh, PA) (1:2) prior to multichannel fluorescence imaging (objectives 5X and 10X) with Zeiss AxioObserver Z1 microscope (Carl Zeiss Microscopy GmbH; Jena, Germany). A custom MATLAB script to measure the spatial position of each invading cell (with center of primary spheroid as coordinate origin) was used as reported previously (13).

PDT and Chemotherapy Treatments:

For PDT treatment, culture media was replaced with media containing 250 nM concentration of verteporfin (BPD, benzoporphyrin derivative monoacid ring A; Sigma-Aldrich; St. Louis, MO), and incubated for 2.5 hours and returned to regular complete media immediately prior to irradiation. A 690 nm laser (Intense; New Brunswick, NJ) was used to excite the photosensitizer, with laser shutter timing controlled by THORLABS APT software to deliver specified total fluence at an irradiance of 100 mW/cm^2. Treatment response was determined 24 hours after treatment. In cultures treated with oxaliplatin (Selleck Chemical; Houston, TX) the drug was added to the media and incubated for 72 hours at which time response was assessed using MATLAB code as described above for quantitative analysis of invasion from fluorescence image fields of 3D spheroids and surrounding invading cells stained with vital dyes, calcein AM and ethidium bromide. For quantification of response in invading cells the large central spheroid (the largest segmented foreground object) is omitted and the number, position and signal from calcein and ethidium bromide for each invading cell are tabulated. For quantification of tumor response in the live signal from the primary nodule is used to estimate tumor volume based on an ellipsoid approximation as described previously (34, 35).

Immunofluorescence Imaging:

Cells in optical-bottom multiwell plates were fixed with 4% formalin, incubated with 0.1% triton X-100 for 20 minutes, and washed three times with 0.1 M glycine. They were refrigerated overnight with primary antibodies against e-cadherin and vimentin (Cell Signaling EMT Duplex; Danvers, MA). After washing with PBS, cells were incubated for 1 hour with mouse or rabbit Alexa Fluor conjugated secondary antibodies (Cell Signaling; Danvers, MA). Cells were mounted with ProLong Gold Antifade reagent with DAPI (ThermoFisher Scientific Molecular Probes; Waltham, MA) and imaged after 24 hours using the same exposure times for all culture conditions on an automated Zeiss AxioObserver Z1 widefield fluorescence microscope. Images were optimized for display in figures using the Hi-Lo lookup table in ImageJ.

RESULTS AND DISCUSSION

Rheology of photocrosslinked COL1

To characterize the change in mechanical properties of COL1 with varying extent of photocrosslinking, hydrogels were prepared in 60mm petri dishes that could be transferred on to the lower plate of an oscillatory shear rheometer after irradiation with blue light. Figure 2A shows the compilation of frequency sweep data for COL1 gels (3.7 mg/mL protein concentration) with RF activated using 450nm light at total fluence from 0 to 100 J/cm^2 with values plotted for $G'(\omega = 20$ rad/s) and $G''(\omega = 20$ rad/s). Full frequency dependence data from which Figure 2A is compiled for each light dose and control groups for light only (at highest dose, 100 J/cm^2) and RF without light are shown in Supplemental Figure 1. As expected there is significant stiffening (increase in the storage modulus, G') with increased light dose, from around 50 Pa at 0 J/cm^2 up to about 160 Pa at 25 J/cm^2. However, at higher light doses we see a drop in modulus such that shear modulus values at 100J/cm^2 are about the same as the initial un-irradiated hydrogel, presumably due to photodestruction caused by excess ROS production beyond the threshold for activating of crosslink formation.

In addition to characterization of linear viscoelastic response we also examined the strength of photocrosslinked hydrogels by gradually increasing oscillatory shear strain past the point of material failure. As seen in Figure 2B the yield strength of the material also peaks in samples that were irradiated with 25 J/cm^2, mirroring the trend in shear modulus plotted above. A representative strain sweep from which Figure 2B data was derived is shown in Supplemental Figure 2.

ECM invasion from transplanted spheroids is regulated by extent of photocrosslinking

Tumor spheroids formed from PANC-1 cells were transplanted in COL1 in solution phase then crosslinked to varying extent to examine how (or if) ECM infiltration by cells at spheroid periphery varies with the degree of crosslinking. Transplanted spheroids were allowed 6 days to grow and invade into the surrounding ECM before terminal fluorescence staining as shown for conditions with no crosslinking (no RF, no light), low extent of crosslinking (RF plus 0.5 J/cm^2) or relatively high extent of crosslinking (RF plus 15 J/cm^2) are shown in Figure 3. For the purposes of this study we define an “invading” cell to be one which has disassociated completely from the primary spheroid transplant such that it is appears as a separate, non-connected foreground object upon image segmentation. As seen in the image data viable (calcein positive) ECM-invading cells can be seen at distances of hundreds of microns away from primary spheroids in the softer uncrosslinked or low crosslinked conditions but not in the collagen which received a 15J/cm^2 fluence of blue light. To quantify these observations, image data from 4 independent experiments (each with triplicates of each collagen condition) were analyzed using an image processing routine to report the number and location of each invading cell relative to the center of its primary spheroid. From tabulated data of invading cell position for each condition, histograms shown in Figure 4A – F were derived and confirm the qualitative observation that in cultures with little or no crosslinking there are higher numbers of viable invading cells at larger distances as compared to highly crosslinked samples with in which invasion is confined to small

numbers of cells close to the edge of the spheroid. This set of observations is reported more compactly in Figure 4G, which shows that invasive velocity (defined as the average distance traversed from the spheroid by the leader cells in each condition, divided by time) decreases monotonically with extent of photocrosslinking.

For further phenotypic analysis cells in invasion promoting (little or no crosslinking, RF without light activation) versus invasion constraining (high crosslinking, RF plus 15 J/cm^2) conditions were stained with EMT markers E-cadherin and Vimentin. As cells undergo EMT and break off from adherens junctions, expression of E-cadherin should decrease while cytoskeletal vimentin should increase concomitant with morphological changes associated with increased motility. In Figure 5, the dramatic increase in cytoskeletal vimentin, elongated protrusions and total absence of E-cadherin in the invading cells in the low-crosslinking conditions are consistent with this trend.

The observation that less invasion is achieved in the more rigid crosslinked COL1 could at first pass appear to be in contradiction to literature which has demonstrated that matrix stiffness promotes invasive behavior (15-17). However, this data suggests that promoting invasive behavior, and actually achieving invasive motility are two different things. While COL1 itself activates invasive behavior (6, 7), and here the COL1 density is the same for each rigidity condition, in this case the more rigid (more highly cross-linked) ECM conditions will also have smaller pore size and likely greater steric hinderance to motility than the softer (less crosslinked) ECM conditions, thus potentially allowing less invasive progression even if increased rigidity tends to promote invasiveness. Another important consideration here is that the changes in stiffness achievable with photocrosslinking prior to the onset of photodegradation and loss of rigidity are relatively small compared to what can be achieved in quasi-2D overlays on synthetic hydrogels which can allow variation of elastic modulus by orders of magnitude. Regardless of the underlying mechanisms, the characterization presented here establishes a set of experimental conditions which can be used to reproducibly promote or constrain invasive behavior in a biologically relevant COL1 ECM microenvironment. Building on this finding, we further leverage this system as a means to study how primary spheroid and invading cell populations respond to treatment.

Assessment of response to chemotherapy and PDT in invasion-promoting versus invasion-constraining COL1 ECM microenvironments

Having established experimental conditions to regulate the extent of ECM invasion in our 3D tumor models we use this approach as the basis for a treatment assessment pipeline shown schematically in Figure 6. For the purpose of treatment assessment experiments we selected the conditions that would produce highly contrasting levels of ECM invasion, using RF-containing COL1 hydrogels with minimal light activation (0.5 J/cm^2) or with a high degree of photocrosslinking (15 J/cm^2).

As shown in Figure 7A, untreated (NT) cultures have either extensive invasion or very limited invasion into ECM in these respective conditions. When treated with verteporfin activated by 690nm light with fluence of 25 J/cm^2 we see strong cytotoxic response in the invasive cells. In the PDT-treated sample with high crosslinking there were few invading cells to begin with but the response to PDT reported as fractional viability (Figure 7B) is

consistent in both ECM environments. In contrast, in the oxaliplatin chemotherapy-treated cultures the invading cells are essentially non-responsive (highly chemoresistant). This is also true with approximately proportional response for the relatively small number of invading cells in the high-crosslinking conditions. The capability of verteporfin PDT to target the ECM infiltrating populations, which also exhibit markers of increased EMT, is potentially significant as this same cell population is not only chemoresistant (as seen here) but also associated with high metastatic potential and poor outcomes (36).

This system also allows us to look at the treatment response of the primary tumor spheroid, expressing the outcome as fraction of tumor volume relative to the respective untreated control in the same ECM environment (Figure 7C). Here we see the opposite trend, in which the primary spheroid exhibits limited response to PDT in terms of volumetric reduction relative to NT control, but the oxaliplatin chemotherapy has a significant growth inhibitory effect. However, even though the oxaliplatin treatment has a greater impact on tumor growth, the spatial pattern of fluorescence staining (Figure 7A) suggests that there is not a strong cytotoxic response, even in cells on the outer periphery of the primary nodules as is the case with PDT. Taken together with the overall trend observed here that invasive populations exhibit the most sensitivity to PDT it may be that the pre-invasive cells at the nodule periphery, or cells with invasive phenotype that have not yet infiltrated into ECM, also exhibit enhanced response to PDT.

Overall this study points to the utility of using COL1 photocrosslinking as a means for tuning rigidity in 3D tumor models independent of ECM protein concentration. As shown here, the ease of controlling RF activation light dose to regulate the extent of crosslinking also leads to reproducible regulation of the degree of invasion by cancer cells. We use this approach in an experimental capacity, to assay the differential therapeutic sensitivity of ECM invading and primary spheroid populations. However, the strong restriction of invasive progression from tumor spheroids also suggests the possibility for therapeutically inhibiting tumor invasion which could be explored further using in vivo models with extent of metastasis as an endpoint. In the context which photocrosslinking is used to regulate invasion here, a significant observation is the ability of PDT to target ECM invading and chemoresistant cancer cells.

Supplementary Material

Refer to Web version on PubMed Central for supplementary material.

ACKNOWLEDGMENTS:

This work was supported by funding from the National Cancer Institute (R00CA155045, to JPC). RJ was supported in part by funding from the UMass Boston/ Dana Farber-Harvard Cancer Center Partnership (U54CA156734). GMC was supported by a Sanofi-Genzyme doctoral research funding while working on this project.

REFERENCES

1. Huang S and Ingber DE (2005) Cell tension, matrix mechanics, and cancer development. Cancer Cell 8, 175–176. [PubMed: 16169461]

2. Lu P, Weaver VM and Werb Z (2012) The extracellular matrix: a dynamic niche in cancer progression. The Journal of cell biology 196, 395–406. [PubMed: 22351925]
3. Paszek MJ, Zahir N, Johnson KR, Lakins JN, Rozenberg GI, Gefen A, Reinhart-King CA, Margulies SS, Dembo M and Boettiger D (2005) Tensional homeostasis and the malignant phenotype. Cancer cell 8, 241–254. [PubMed: 16169468]
4. Kalluri R and Zeisberg M (2006) Fibroblasts in cancer. Nature Reviews Cancer 6, 392–401. [PubMed: 16572188]
5. Nguyen-Ngoc K-V, Cheung KJ, Brenot A, Shamir ER, Gray RS, Hines WC, Yaswen P, Werb Z and Ewald AJ (2012) ECM microenvironment regulates collective migration and local dissemination in normal and malignant mammary epithelium. Proceedings of the National Academy of Sciences 109, E2595–E2604.
6. Shields MA, Dangi-Garimella S, Krantz SB, Bentrem DJ and Munshi HG (2011) Pancreatic Cancer Cells Respond to Type I Collagen by Inducing Snail Expression to Promote Membrane Type 1 Matrix Metalloproteinase-dependent Collagen Invasion. Journal of Biological Chemistry 286, 10495–10504. [PubMed: 21288898]
7. Shintani Y, Hollingsworth MA, Wheelock MJ and Johnson KR (2006) Collagen I Promotes Metastasis in Pancreatic Cancer by Activating c-Jun NH2-Terminal Kinase 1 and Up-regulating N-Cadherin Expression. Cancer Research 66, 11745–11753. [PubMed: 17178870]
8. Bardeesy N and DePinho RA (2002) Pancreatic cancer biology and genetics. Nature Reviews Cancer 2, 897–909. [PubMed: 12459728]
9. Feig C, Gopinathan A, Neesse A, Chan DS, Cook N and Tuveson DA (2012) The Pancreas Cancer Microenvironment. Clinical Cancer Research 18, 4266–4276. [PubMed: 22896693]
10. Whatcott CJ, Diep CH, Jiang P, Watanabe A, LoBello J, Sima C, Hostetter G, Shepard HM, Von Hoff DD and Han H (2015) Desmoplasia in primary tumors and metastatic lesions of pancreatic cancer. Clinical Cancer Research 21, 3561–3568. [PubMed: 25695692]
11. Ulrich TA, Jain A, Tanner K, MacKay JL and Kumar S (2010) Probing cellular mechanobiology in three-dimensional culture with collagen–agarose matrices. Biomaterials 31, 1875–1884. [PubMed: 19926126]
12. Rice A, Cortes E, Lachowski D, Cheung B, Karim S, Morton J and Del Rio Hernandez A (2017) Matrix stiffness induces epithelial–mesenchymal transition and promotes chemoresistance in pancreatic cancer cells. Oncogenesis 6, e352. [PubMed: 28671675]
13. Cramer GM, Jones DP, El-Hamidi H and Celli JP (2017) ECM Composition and Rheology Regulate Growth, Motility, and Response to Photodynamic Therapy in 3D Models of Pancreatic Ductal Adenocarcinoma. Mol Cancer Res 15, 15–25. [PubMed: 27671335]
14. Alessandri K, Sarangi BR, Gurchenkov VV, Sinha B, Kießling TR, Fetler L, Rico F, Scheuring S, Lamaze C and Simon A (2013) Cellular capsules as a tool for multicellular spheroid production and for investigating the mechanics of tumor progression in vitro. Proceedings of the National Academy of Sciences 110, 14843–14848.
15. Celli JP and Anderson MD (2017) Cancer Biophysics In Reference Module in Life Sciences. Elsevier.
16. Acerbi I, Cassereau L, Dean I, Shi Q, Au A, Park C, Chen YY, Liphardt J, Hwang ES and Weaver VM (2015) Human breast cancer invasion and aggression correlates with ECM stiffening and immune cell infiltration. Integrative Biology 7, 1120–1134. [PubMed: 25959051]
17. Wei SC, Fattet L, Tsai JH, Guo Y, Pai VH, Majeski HE, Chen AC, Sah RL, Taylor SS, Engler AJ and Yang J (2015) Matrix stiffness drives epithelial–mesenchymal transition and tumour metastasis through a TWIST1–G3BP2 mechanotransduction pathway. Nature Cell Biology 17, 678. [PubMed: 25893917]
18. Zaman MH, Trapani LM, Sieminski AL, MacKellar D, Gong H, Kamm RD, Wells A, Lauffenburger DA and Matsudaira P (2006) Migration of tumor cells in 3D matrices is governed by matrix stiffness along with cell-matrix adhesion and proteolysis. Proceedings of the National Academy of Sciences 103, 10889–10894.
19. Soman P, Kelber JA, Lee JW, Wright TN, Vecchio KS, Klemke RL and Chen S (2012) Cancer cell migration within 3D layer-by-layer microfabricated photocrosslinked PEG scaffolds with tunable stiffness. Biomaterials 33, 7064–7070. [PubMed: 22809641]

20. Gill BJ, Gibbons DL, Roudsari LC, Saik JE, Rizvi ZH, Roybal JD, Kurie JM and West JL (2012) A synthetic matrix with independently tunable biochemistry and mechanical properties to study epithelial morphogenesis and EMT in a lung adenocarcinoma model. Cancer research 72, 6013–6023. [PubMed: 22952217]
21. Ananthanarayanan B, Kim Y and Kumar S (2011) Elucidating the mechanobiology of malignant brain tumors using a brain matrix-mimetic hyaluronic acid hydrogel platform. Biomaterials 32, 7913–7923. [PubMed: 21820737]
22. Cherfan D, Verter EE, Melki S, Gisel TE, Doyle FJ, Scarcelli G, Yun SH, Redmond RW and Kochevar IE (2013) Collagen Cross-Linking Using Rose Bengal and Green Light to Increase Corneal StiffnessCollagen Cross-Linking to Augment Corneal Stiffness. Investigative ophthalmology & visual science 54, 3426–3433. [PubMed: 23599326]
23. Hafezi F, Kanellopoulos J, Wiltfang R and Seiler T (2007) Corneal collagen crosslinking with riboflavin and ultraviolet A to treat induced keratectasia after laser in situ keratomileusis. Journal of Cataract & Refractive Surgery 33, 2035–2040. [PubMed: 18053900]
24. Mencucci R, Marini M, Paladini I, Sarchielli E, Sgambati E, Menchini U and Vannelli GB (2010) Effects of riboflavin/UVA corneal cross-linking on keratocytes and collagen fibres in human cornea. Clinical & experimental ophthalmology 38, 49–56. [PubMed: 20447101]
25. Brennan-Pierce EP, MacAskill I, Price RB and Lee JM (2014) Riboflavin-sensitized photo-crosslinking of collagen using a dental curing light. Bio-medical materials and engineering 24, 1659–1671. [PubMed: 24948451]
26. Grobe GM and Reichl S (2011) Examining the suitability of riboflavin/UVA treatment for strengthening the stromal bioequivalent of a human cornea construct. Current eye research 36, 217–231. [PubMed: 21275608]
27. Ibusuki S, Halbesma GJ, Randolph MA, Redmond RW, Kochevar IE and Gill TJ (2007) Photochemically cross-linked collagen gels as three-dimensional scaffolds for tissue engineering. Tissue engineering 13, 1995–2001. [PubMed: 17518705]
28. Conroy T, Desseigne F, Ychou M, Bouché O, Guimbaud R, Bécouarn Y, Adenis A, Raoul J-L, Gourgou-Bourgade S and de la Fouchardière C (2011) FOLFIRINOX versus gemcitabine for metastatic pancreatic cancer. New England Journal of Medicine 364, 1817–1825. [PubMed: 21561347]
29. Huggett MT, Jermyn M, Gillams A, Illing R, Mosse S, Novelli M, Kent E, Bown S, Hasan T and Pogue B (2014) Phase I/II study of verteporfin photodynamic therapy in locally advanced pancreatic cancer. British journal of cancer 110, 1698. [PubMed: 24569464]
30. Wollensak G, Spoerl E, Wilsch M and Seiler T (2004) Keratocyte apoptosis after corneal collagen cross-linking using riboflavin/UVA treatment. Cornea 23, 43–49. [PubMed: 14701957]
31. Baiocchi S, Mazzotta C, Cerretani D, Caporossi T and Caporossi A (2009) Corneal crosslinking: riboflavin concentration in corneal stroma exposed with and without epithelium. Journal of Cataract & Refractive Surgery 35, 893–899. [PubMed: 19393890]
32. Ibusuki S, Papadopoulos A, Ranka MP, Halbesma GJ, Randolph MA, Redmond RW, Kochevar IE and Gill TJ (2009) Engineering cartilage in a photochemically crosslinked collagen gel. Journal of Knee Surgery 22, 72–81. [PubMed: 19216355]
33. Jones D, Hanna W, El-Hamidi H and Celli J (2014) Longitudinal Measurement of Extracellular Matrix Rigidity in 3D Tumor Models Using Particle-tracking Microrheology. J Vis Exp 88.
34. Celli JP, Rizvi I, Blanden AR, Massodi I, Glidden MD, Pogue BW and Hasan T (2014) An imaging-based platform for high-content, quantitative evaluation of therapeutic response in 3D tumour models. Scientific reports 4, 3751. [PubMed: 24435043]
35. Anbil SR, Rizvi I, Celli JP, Alagic N, Pogue BW and Hasan T (2013) Impact of treatment response metrics on photodynamic therapy planning and outcomes in a three-dimensional model of ovarian cancer. Journal of Biomedical Optics 18, 098004. [PubMed: 24802230]
36. Singh A and Settleman J (2010) EMT, cancer stem cells and drug resistance: an emerging axis of evil in the war on cancer. Oncogene 29, 4741. [PubMed: 20531305]

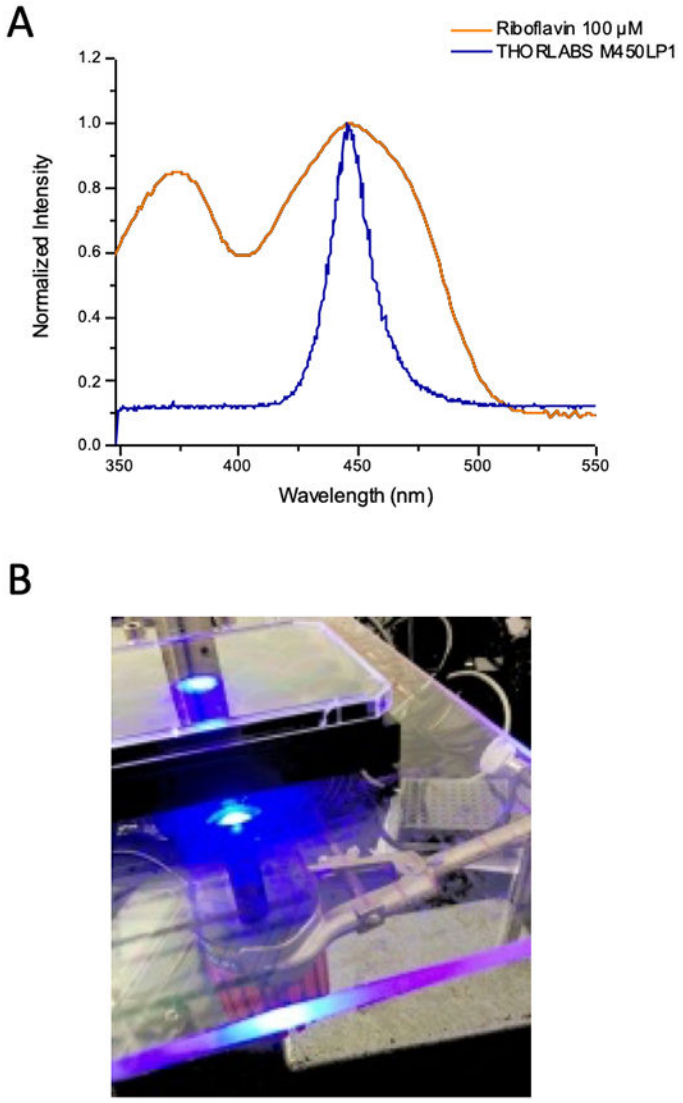

Figure 1.

A) Emission spectrum of light source used for photocrosslinking experiments in this study overlaid on measured UV-Vis absorption spectrum for riboflavin. B) Photograph of photocrosslinking light delivery setup for multiwell plates used in cell culture experiments.

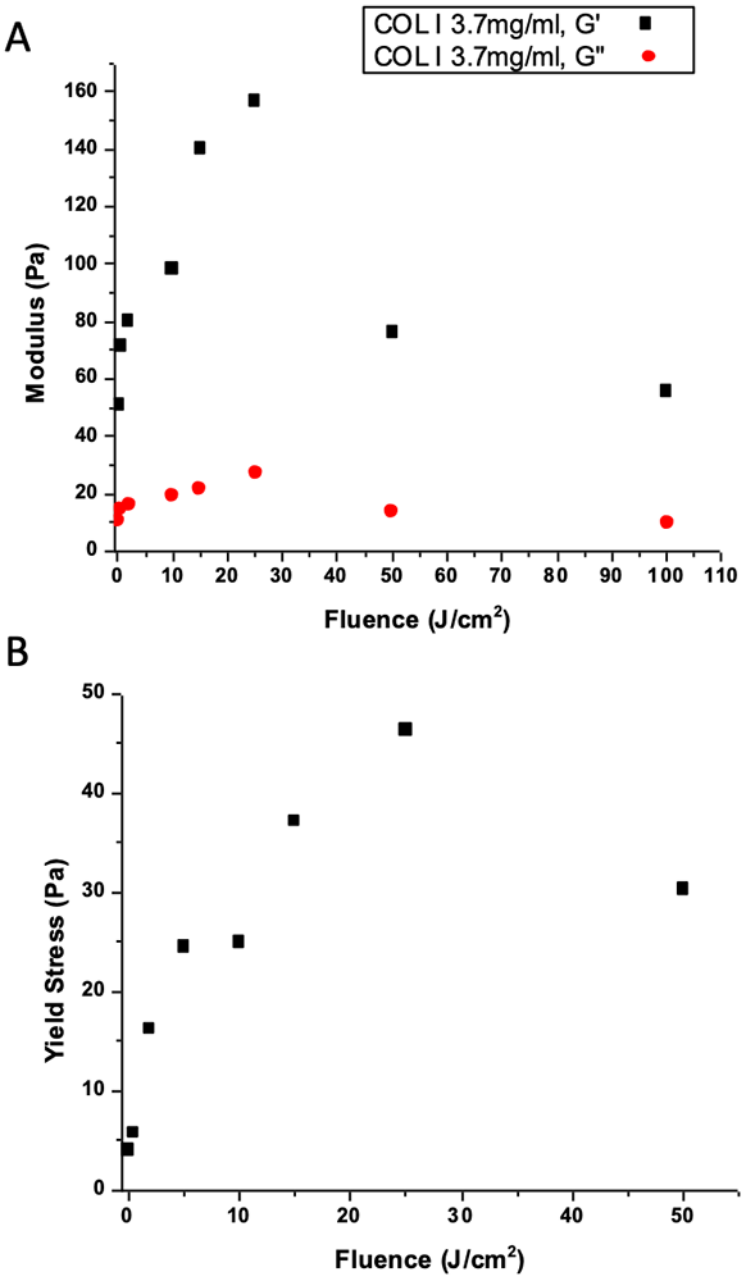

Figure 2.

Oscillatory shear rheology characterization of COL1 hydrogels with varying extent of photocrosslinking and control samples. A) Measurement of storage and loss moduli for each ECM condition. Values shown are for angular frequency of 20 rad/s, obtained from full frequency sweeps (Supplementary Figure 1). Hydrogel stiffness increases up to a blue light dose of about 25 J/cm^2, above which photodegradation effects become significant and matrix stiffness decreases. B) COL1 yield stress as a function of crosslinking is consistent with the above data, showing increasing mechanical strength with light dose up to about 25 J/cm^2.

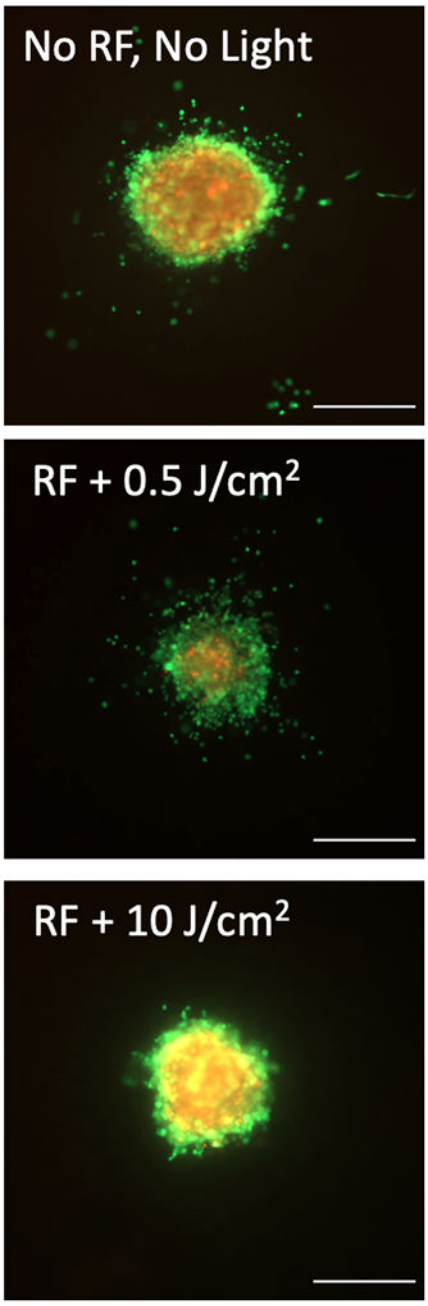

Figure 3.

Representative fluorescence images of tumor spheroids transplanted into hydrogels with no photocrosslinking (no RF, no light, top), a low photocrosslinking light dose (RF plus 0.5 J/cm^2, middle), or relatively high photocrosslinking light dose (RF plus 10J/cm^2) and stained with vital dyes, calcein AM (green, live cells) and ethidium bromide (red, dead cells). The number of invading cells, and their distance from the primary spheroid decreases as the extent of crosslinking (and matrix stiffness) increases. Scale bars = 500μm.

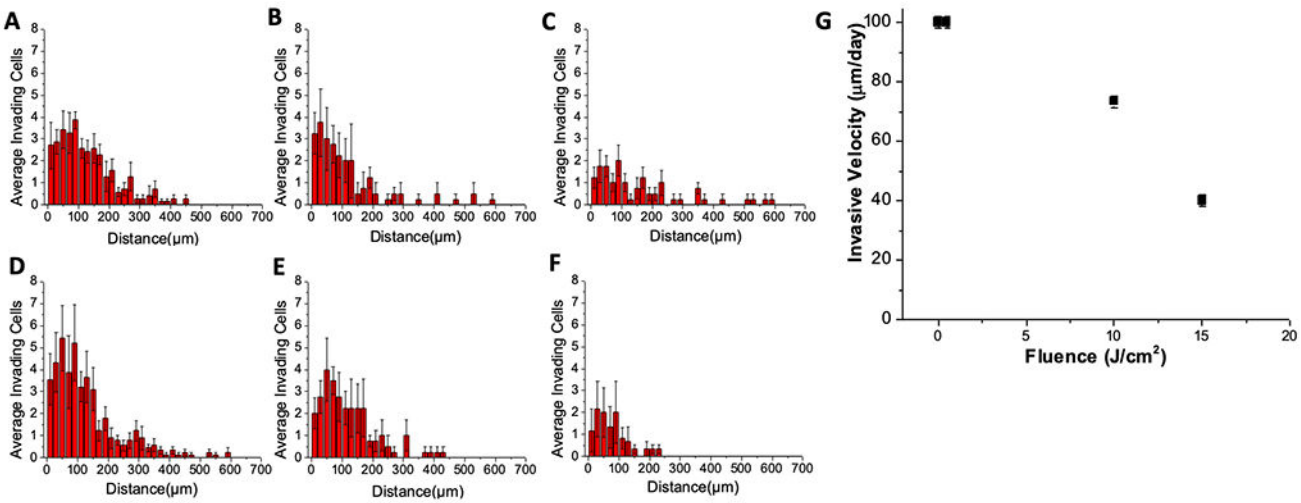

Figure 4.

Histograms derived from quantitative image processing of the extent of ECM invasion in all replicate image fields for each photocrosslinking and control condition for batch-processed image data of spheroid transplants in COL1 with: A) Light only (15 J/cm^2 from 450nm LED source) B) No light, No RF, C) RF only (no light), D) RF with 0.5 J/cm^2 E) RF plus 10 J/cm^2, and F) RF plus 15 J/cm^2. In G) the invasive velocity (distance invaded by leader cells from primary nodule divided by time) is plotted against light dose (where 0 J/cm2 corresponds to RF only) showing monotonic decrease with extent of cross-linking.

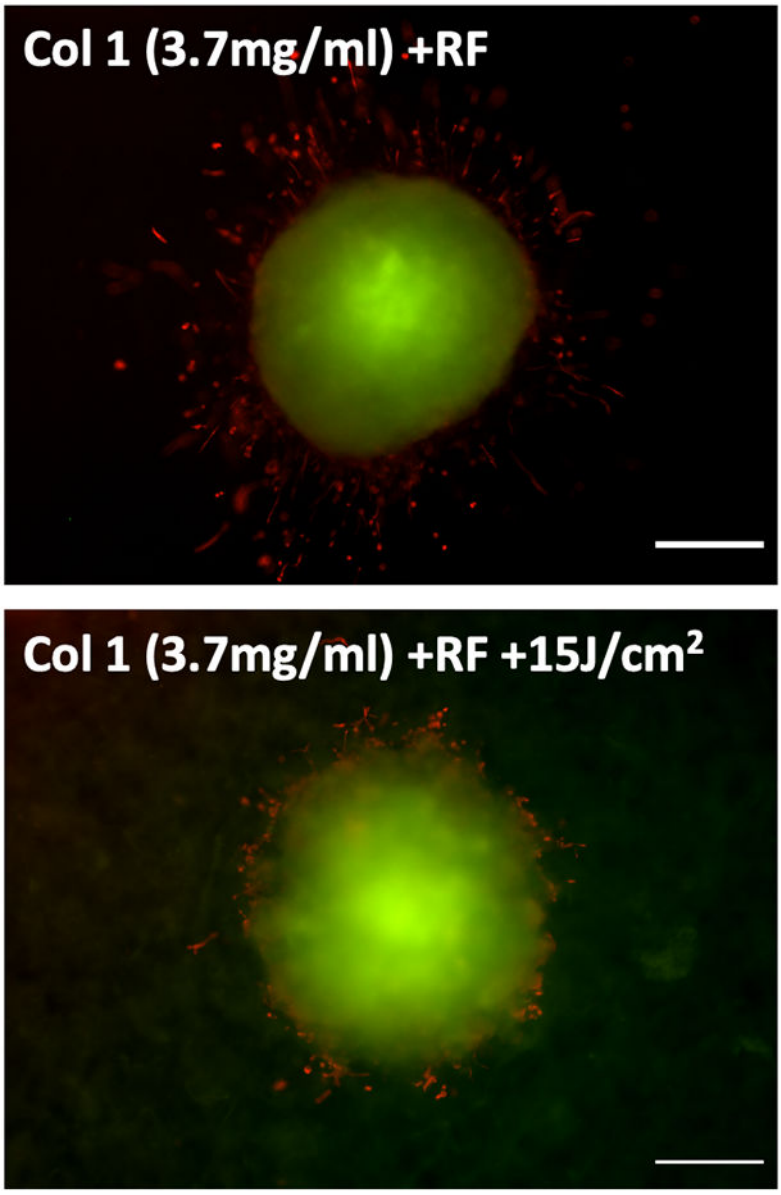

Figure 5.

Immunofluorescence imaging of spheroid transplants in COL1 hydrogels with no photocrosslinking (RF only, upper panel) or extensive photocrosslinking (RF plus 15 J/cm^2, lower panel) stained using antibodies against E-cadherin (green) and vimentin (red). Invading cells exhibit elongated protrusions, strong vimentin and absence of E-cadherin staining. Scale bars = 200 μm.

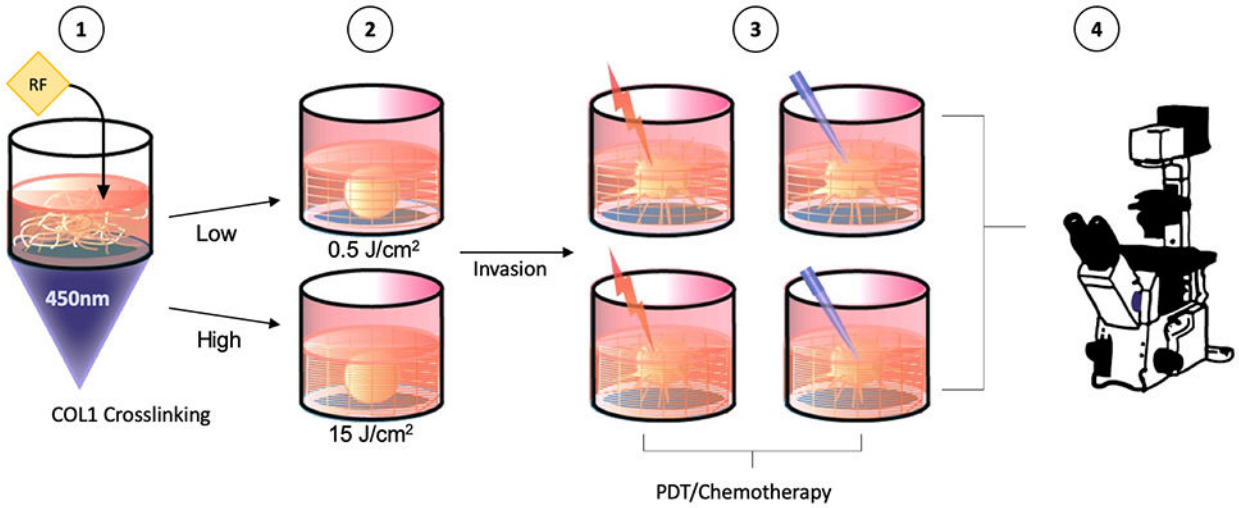

Figure 6.

Schematic representation of workflow for chemotherapy and PDT treatment assessment experiments in COL1 with low (0.5 J/cm^2) and high (15 J/cm^2) photocrosslinking.

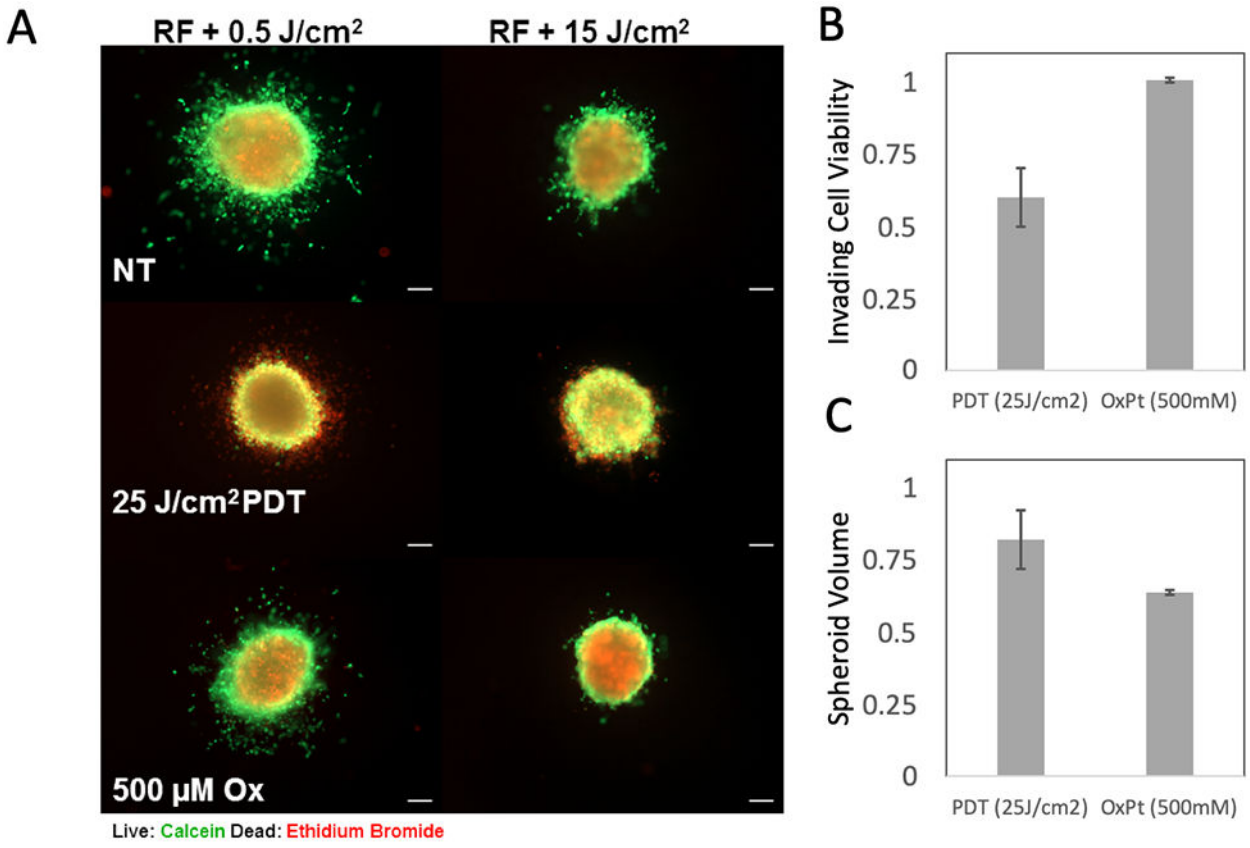

Figure 7.

Response to verteporfin PDT and oxaliplatin (Ox) chemotherapy in COL1 environments with high and low photocrosslinking. Fluorescence images in A) show representative transplanted spheroids receiving no treatment (NT), verteporfin activated by 690nm light at 25J/cm^2 or 500µM oxaliplatin, in COL1 with RF exposed to 0.5 J/cm^2 (left panels) or 15 J/cm^2 (right panels). Panel B) shows quantitative assessment of invading cell fields (from COL1 with low crosslinking). Treatment response of invading cells (reported as number of viable invading cells divided by total, relative to NT control) shows significant chemoresistance, yet sensitivity to PDT in this populations ($p = 0.016$, two-tailed student's t-test). This analysis is based on image-segmentation which excludes the primary spheroid and quantifies live and dead invading cells only. Panel C) shows residual viable tumor volume for PDT and chemotherapy treated primary spheroids (in high-crosslinking invasion-suppressing COL1 conditions). Here, greater growth inhibition of primary spheroids is achieved with oxaliplatin chemotherapy relative to verteporfin PDT.